University of Texas Rio Grande Valley

ScholarWorks @ UTRGV

Electrical and Computer Engineering Faculty Publications and Presentations

College of Engineering and Computer Science

1-25-2022

Investigation of the Effect and Contribution of Process Parameters By Taguchi and ANOVA Analysis on the Morphological and Electrical Properties of RF Magnetron Sputtered SiO2 Over Si Substrate

Sajid Mahfuz Uchayash
The University of Texas Rio Grande Valley

Prosanto Biswas
The University of Texas Rio Grande Valley

Meah Imtiaz Zulkarnain
The University of Texas Rio Grande Valley

Ahmed Touhami
The University of Texas Rio Grande Valley, ahmed.touhami@utrgv.edu

Nazmul Islam
The University of Texas Rio Grande Valley, nazmul.islam@utrgv.edu

Follow this and additional works at: https://scholarworks.utrgv.edu/ece_fac

Part of the Electrical and Computer Engineering Commons

See next page for additional authors

Recommended Citation

Uchayash, SM, Biswas, P, Zulkarnain, MI, Touhami, A, Islam, N, & Huq, H. "Investigation of the Effect and Contribution of Process Parameters By Taguchi and ANOVA Analysis on the Morphological and Electrical Properties of RF Magnetron Sputtered SiO2 Over Si Substrate." Proceedings of the ASME 2021 International Mechanical Engineering Congress and Exposition. Volume 3: Advanced Materials: Design, Processing, Characterization, and Applications. Virtual, Online. November 1–5, 2021. V003T03A039. ASME. https://doi.org/10.1115/IMECE2021-73849

This Conference Proceeding is brought to you for free and open access by the College of Engineering and Computer Science at ScholarWorks @ UTRGV. It has been accepted for inclusion in Electrical and Computer Engineering Faculty Publications and Presentations by an authorized administrator of ScholarWorks @ UTRGV. For more information, please contact justin.white@utrgv.edu, william.flores01@utrgv.edu.

Authors

Sajid Mahfuz Uchayash, Prosanto Biswas, Meah Imtiaz Zulkarnain, Ahmed Touhami, Nazmul Islam, and Hasina Huq

This conference proceeding is available at ScholarWorks @ UTRGV: https://scholarworks.utrgv.edu/ece_fac/55

Check for updates

Proceedings of the ASME 2021
International Mechanical Engineering Congress and Exposition
IMECE2021
November 1-5, 2021, Virtual, Online

IMECE2021-73849

Downloaded from http://asmedigitalcollection.asme.org/IMECE/proceedings-pdf/IMECE2021/85574/V003T03A039/6827069/v003t03a039-imece2021-73849.pdf by Texas A & M University user on 23 January 2023

INVESTIGATION OF THE EFFECT AND CONTRIBUTION OF PROCESS PARAMETERS BY TAGUCHI AND ANOVA ANALYSIS ON THE MORPHOLOGICAL AND ELECTRICAL PROPERTIES OF RF MAGNETRON SPUTTERED SiO_2 OVER Si SUBSTRATE

Sajid Mahfuz Uchayash
Department of ECE
UTRGV, Edinburg, TX

Prosanto Biswas
Department of ECE
UTRGV, Edinburg, TX

Meah Imtiaz Zulkarnain
Department of ECE
UTRGV, Edinburg, TX

Ahmed Touhami
Department of Physics
UTRGV, Brownsville, TX

Nazmul Islam
Department of ECE
UTRGV, Edinburg, TX

Hasina Huq
Department of ECE
UTRGV, Edinburg, TX

ABSTRACT

In this work, we applied Taguchi Signal-to-noise (S/N) analysis to investigate the effect of varying three process parameters, namely- sputtering power, working pressure and Ar gas flow rate on the surface, morphological and electrical properties of the RF sputtered SiO_2 over Si substrate. We also inspected the contribution of a particular process parameter on these properties by applying Analysis of Variance (ANOVA). SiO_2 thin films were fabricated over Si substrate using RF magnetron sputtering system. Three sets of inputs for the three mentioned process parameters were chosen; for power, we chose 100W, 150W and 200W; 5mTorr, 10mTorr and 15mTorr were chosen for pressure and three Ar gas flow rate levels at 5, 10 and 15 sccm were selected. By performing Taguchi L^9 orthogonal array, nine combinations of sputtering parameters were prepared for depositing SiO_2/Si Thin films. The surface morphological and electrical properties (resistivity per unit area and capacitance per unit area) of the sputtered samples were therefore inspected by analyzing the Taguchi design of experiment. Signal-to-noise (S/R) analysis presents how the properties were affected by the variation of each process parameter. ANOVA analysis showed that sputtering power and working pressure are the two dominant process parameters contributing more to surface morphological and electrical properties. A regression model for surface roughness of the SiO_2/Si thin film samples was also derived. The electrical properties of the SiO_2/Si thin films, however, didn't show linear properties.

Keywords: Sputtering system, SiO_2 thin film, Taguchi analysis, impedance spectroscopy.

NOMENCLATURE

SiO_2/Si	SiO_2 thin film over Si substrate
DOE	Design of experiments
sccm	Standard cubic cm per minute
S/N	Signal to Noise Ratio
DF	Degrees of Freedom
Seq SS	Sequential sum of squares
Adj SS	Adjusted sum of squares
Adj MS	Adjusted mean of squares
R^2 (adj)	R^2 adjusted
R^2 pred)	R^2 predicted
R_a	Average surface roughness
R_{nA}	Resistance/Area of nth SiO_2/Si samples
C_{nA}	Capacitance/Area of nth SiO_2/Si samples
R_{Si}	Resistance of the Si Substrate
C_{Si}	Capacitance of the Si Substrate
R_{nSiO_2}	Resistance of the nth SiO_2 film
C_{nSiO_2}	Resistance of the nth SiO_2 film
R_n	Resistance of nth SiO_2/Si samples
C_n	Capacitance of nth SiO_2/Si samples
Z_n (r)	Real part of impedance of nth sample
Z_n (i)	Imaginary part of impedance of nth sample
d_n	Layer thickness of nth sample
d_{Si}	Layer thickness the Si substrate
A_n	Area of the nth thin film sample

Copyright © 2021 by ASME

1. INTRODUCTION

Thin films of SiO_2 have a broad range of usage in microelectronics, MEMS and optoelectronic devices. For example- as diffusion masks and passivation coating, SiO_2 thin films are widely used in Si-based IC [1, 2]. In MEMS, apart from general use as structural or sacrificial layer [3-5], deposited SiO_2 thin films are the focus of interest to realize suspended microstructure like cantilever beams and micro-bridge [6]. In optoelectronic devices like solar cells, due to their adaptivity to harsh environments [7] and transparency [8], SiO_2 thins films, often in combination with other oxide thin films. are used as anti-reflection and absorption coating [7-11]. The use of SiO_2 films as gate insulation layer in CMOS technology is universal. Dynamic Random Access Memory (DRAM) and Resistance Switching Random Access Memory (ReRAM) use SiO_2 layer as capacitor dielectrics [12, 13]. In detector/sensor applications, or for solar energy devices SiO_2 layer works as intermetal insulator. Compound thin films of transition metal and metal oxides with SiO_2 increase the dielectric constant of the layer, which reduces leakage current and improves device properties [14].

Despite having a low deposition rate, RF magnetron sputtering offers the following advantages over the commonly used oxidation at high temperature and Chemical Vapor Deposition (CVD) method for fabricating oxide thin films - low cost, less complexity, the flexibility of sequential deposition, elimination of toxic gases, uniform deposition at larger areas and protection of microelectronic circuits from higher temperature [15, 16]. SiO_2 thin film deposited by magnetron sputtering has been reported in several previous works [15-19], many of which investigated the structural, electrical and insulation characteristics of the sputtered SiO_2 thin films as the function of the process parameters. The effect of RF power and working pressure on the deposition rate, O/Si ratio of the film, surface morphology and microstructure was explored in [6, 7]. Electrical properties like- breakdown field strength, resistivity and dielectric constant of the sputtered SiO_2 layer prepared by reactive pulse magnetron sputtering were reported in [12, 17]. Ho et al. studied the conductivity, reverse saturation-current and conversion efficiency of the GaAs solar cell coated with SiO_2 ARC (anti-reflection coating) [12]. For high dielectric strength, layered Al_2O_3-SiO_2 thin film composites deposited by pulsed DC and RF magnetron sputtering were reported by Hanby et al. [18].

In this current work, a detailed study of the effect of process parameters on the surface, structural and electrical properties of SiO_2 thin films deposited on pure Si substrate using RF magnetron sputtering is presented. To investigate the effect of process parameters, we applied the Taguchi design of experiments. Unlike traditional experiments, which may require a large number of samples to experiment with, the Taguchi method provides a systematic design approach with more efficiency using a lesser number of experimental results [20, 21]. Signal to noise ratio (S/N) analysis is applied to understand how the properties of SiO_2/Si thin films vary with the change of three major process parameters- RF sputtering power, working pressure and Ar gas flow rate. Analysis of variance, followed by the S/N result, tells us how much each process parameter contributes to a particular property of the SiO_2/Si thin film. For measuring electrical properties of SiO_2/Si thin film samples- resistivity per unit area (R_{nA}) and capacitance per unit area (C_{nA}), we used Impedance spectroscopy. Using impedance spectroscopy to understand the electrical properties of thin films has been reported in many previous studies [22-25]. Whereas Bartzsch et al. measured the DC/AC resistivity and dielectric constant [12, 17], we varied the frequency from 1Hz to 1MHz and observed the variation of R_{nA} and C_{nA} of the SiO2/Si thin films. A particular frequency where the R_{nA} and C_{nA} of the SiO2/Si thin films show outliers and more trending data was chosen to perform S/N and ANOVA analysis to implement the Taguchi analysis for understanding the effect of parameter changes on resistivity and capacitance of the SiO2/Si thin films. From our data, a regression model for only surface roughness was possible to derive. Electrical properties of SiO_2/Si thin film samples- resistivity per unit area (R_{nA}) and capacitance per unit area (C_{nA}) did not show a linear outcome, and therefore, it was not possible to derive a regression model for these properties.

2. EXPERIMENT AND METHODOLOGY

2.1 Experimental Setup

A 2” diameter 0.125” thick 99.995% pure SiO_2 target was used to create thin films over pure Si (100) substrate (thickness 525±10 μm). Before sputtering, substrates were cleaned with deionized water, Acetone (CH_3-CO-CH_3), Ethanol (C_2H_5OH) and again with DI water and finally blow-dried. The main chamber of the sputtering system (AJA ATC Orion 5 UHV) was vacuumed to the scale 10^{-6} Torr to initiate the process. Three sets of RF power (150, 200 & 250W), pressure (10, 15 & 20 mTorr) and Ar gas flow rate (5, 10 & 15 sccm) were chosen as process parameters for sputtering. 3 level Taguchi design of experiment was applied to create a L^9 (3^3) orthogonal array, which has three columns and nine rows- shown in Table 3. Here the fourth column of the L^9 orthogonal array is left vacant for error of experiments [21], as orthogonality is not affected If one column of the array is empty [26, 27].

RF power was supplied to the sputtering system by 0313 GTC power source, which has a frequency of 13.56MHz. SiO_2 target was pre-sputtered for 30 mins before commencing the sputtering process. The substrate was being rotated at a constant speed of 36rpm to ensure uniformity of the epitaxial growth. The whole process was remotely monitored by software and the impedance matching network was automatically controlled by an auto-tuner (AIT 600 RF). Each sample was sputtered for 3 hr.

The roughness of the sputtered SiO_2/Si thin films was measured by Mahr Marsurf 300 C profilometer. XRD analysis was done by Rigaku Miniflex benchtop X-ray diffractometer using a Cu-Kα source of wavelength 1.5406 A° (30KV, 15mA). Surface and cross-sectional micrographs were obtained by scanning electron microscope (Carl Zeiss, Sigma VP). Surface topographic images were obtained using atomic force microscopy (Bruker Bioscope Catalyst). A potentiostat

Downloaded from http://asmedigitalcollection.asme.org/IMECE/proceedings-pdf/IMECE2021/85574/V003T03A039/6827069/v003t03a039-imece2021-73849.pdf by Texas A & M University user on 23 January 2023

Copyright © 2021 by ASME

(Metrohm Autolab PGSTAT302N) was used for impedance spectroscopy of the SiO_2/Si thin films. Adhesion of the sputtered thin films was performed by scotch tape test. Statistical analysis-Taguchi DOE, ANOVA and regression model were performed in Minitab software.

Table 1: Summary of sputtering process for SiO_2/Si thin films

Substrate	pure Si (100), thickness 525±10 µm
Target	SiO_2, diameter -2", thickness-0.125", purity- 99.995%
Process Gas	Ar, 99.99% purity
Base Pressure	10^{-6} Torr scale
RF Power Source	13.56 MHz (0313 GTC)
Rotation Speed	36 rpm

Table 2: Sputtering parameters for SiO_2/Si thin films

Level	Sputtering parameter	1	2	3
A	RF Power (W)	150	200	250
B	Pressure (mTorr)	10	15	20
C	Ar flow rate (sccm)	5	10	15

Table 3: 9 Sets of parameter combinations from Taguchi L^9 orthogonal array

Sample number	Control factors		
	Power (W) (A)	Pressure (mTorr) (B)	Ar flow rate (sccm) (C)
Sample 1	150 (1)	10 (1)	5 (1)
Sample 2	150 (1)	15 (2)	10 (2)
Sample 3	150 (1)	20 (3)	15 (3)
Sample 4	200 (2)	10 (1)	10 (2)
Sample 5	200 (2)	15 (2)	15 (3)
Sample 6	200 (2)	20 (3)	5 (1)
Sample 7	250 (3)	10 (1)	15 (3)
Sample 8	250 (3)	15 (2)	5 (1)
Sample 9	250 (3)	20 (3)	10 (2)

2.1 Statistical Analysis

Taguchi DOE and S/N ratio: Implementing the theory of experimental design and loss function concept, Taguchi design of experiments provides a robust design model [20, 21]. S/N ratio is the most important analysis of Taguchi design. Signals are the controllable process parameters, whereas noise is something we have no control over during production or product use but can be controlled during experimentation. Two types of S/N ratio analysis are applied here-the smaller the better (for surface roughness) and the higher the better (for R_{ASiO_2} and C_{ASiO_2}).

The formula for the smaller-is-better S/N ratio:

$$\frac{S}{N} = -10 \times \log\left(\left(\sum (Y^2)\right)/n \right) \tag{1}$$

The formula for the larger-is-better S/N ratio:

$$\frac{S}{N} = -10 \times \log\left(\left(\sum \frac{1}{Y^2}\right)/n \right) \tag{2}$$

Where Y is responses for the given factor level combination and n is the number of responses in the factor level combination [28].

Analysis of variance (ANOVA): ANOVA was performed to find out which sputtering parameter has a statistically significant effect over a particular output. Two important calculation regarding ANOVA analysis is F-value and P-value, which indicates the corresponding parameter having a significant impact on response characteristics. F value indicates if the means between two populations are significantly different. If F is large, the variability between treatments is large relative to the variation within treatments, and we reject the null hypothesis of equal means.

$$F = \frac{Variance\ between\ Treatments}{Variance\ within\ Treatments} \tag{3}$$

To determine whether any of the differences between the means are statistically significant, a significant level (α)-indicating a 100α% risk of concluding that a difference exists when there is no actual difference in treatment-is chosen. If the P-value ≤ α, then it means the differences between some of the means are statistically significant.

The following equations were used for ANOVA and F-test of the experimental data [21]:

$$\begin{aligned} S_{mean} &= \frac{(\sum x_i)^2}{n} & S_{Error} &= S_{TV} - \sum S_p \\ S_{TV} &= \sum x_i^2 - S_{mean} & V_p &= \frac{S_p}{f_p} \\ S_p &= \frac{(\sum x_p^2)^2}{n_{rpt}} - S_{mean} & F_p &= \frac{V_P}{V_{Error}} \end{aligned} \tag{4}$$

Where the total number of experiments is N, x_i denotes the output of each experiment, S_{mean} is the sum of squares due to the means, S_{TV} means the sum of square due to the total variation, S_p stands for sum of square due to a parameter, x_p is the sum of the ith level of a parameter (here i=1,2,3), f_p degree of freedom of parameter P, V_p the variance of parameter P and F_p is the F-value of parameter P.

Regression Analysis: The purpose of regression analysis is to generate an equation that describes the relationship between the dependent and independent variables and can predict a new observation.

A general first-order regression equation can be expressed as follows-

$$y = \beta_0 + \sum_{i=1}^{k} \beta_i x_i + \varepsilon \tag{5}$$

Where β represents the coefficient of each term, k is the number of independent variables and the error is designated by ε.

Downloaded from http://asmedigitalcollection.asme.org/IMECE/proceedings-pdf/IMECE2021/85574/V003T03A039/6827069/v003t03a039-imece2021-73849.pdf by Texas A & M University user on 23 January 2023

Copyright © 2021 by ASME

Short description of notation used in regression analysis is given below [29]:

S calculates the deviation of distances of the data values from the fitted values.

R^2 denotes the variation of the actual response from the fitted model.

R^2(adj) adjusts the statistic based on the number of independent variables in the model.

R^2(pred) predicts the efficiency of the model for a new observation.

3. RESULTS AND DISCUSSION

3.1 Roughness

Surface roughness for sputtered SiO_2 thin film is important; for optoelectronic devices where these thin films are used as anti-reflection coating, rough surface will cause more scattering of light and henceforth will decrease the efficiency of the device. Roughness is the result of micro-voids and pores on the sputtered thin-film surface. The average surface roughness R_a for the sputtered SiO_2/Si thin film samples is listed in Table 4. Figure 1 shows the S/N graph for the surface roughness. As it can be seen, roughness increased when working pressure was increased but decreased with increasing power, which agrees well with the theory. When the power is high, the process gas atoms bombard against the target with high kinetic energy- this high energy bombardment, known as atomic peening [6, 30]. Atomic peening excites the falling target atoms, generates more nucleation sites and therefore forming a densely packed structure, filling up most

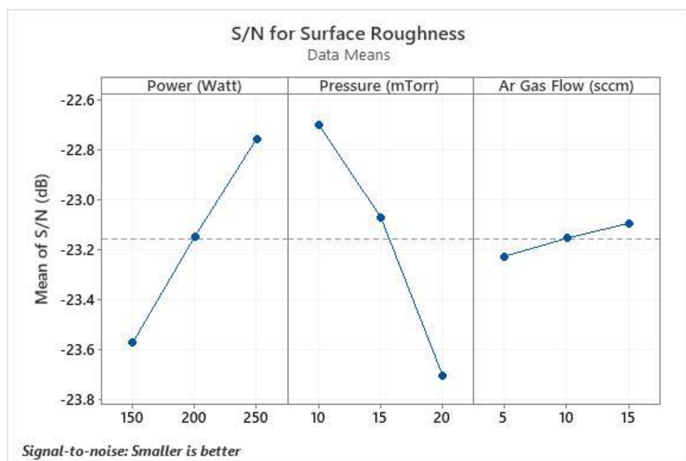

FIGURE 1: S/N RESPONSE GRAPH FOR SURFACE ROUGHNESS OF SiO_2/Si THIN FILMS

of the micro-voids and pores on the surface. Working pressure, on the other hand, has the opposite effect. Higher pressure means less mean free path, so the interatomic collisions between the process gas atoms and falling target atoms diminish the average kinetic energy. A loosely packed structure with high porosity builds up over the substrate as a result. From the analysis of variance of our data, we can conclude that the contribution of pressure is dominant (60.04%) to the surface roughness compared to the working pressure (37.88%). Although from Figure 1, we observed that roughness decreases when Ar gas flow rate is increased, which agrees with previous work [31], ANOVA result however showed that this contribution is not significant at all (P-value > 0.05).

Table 4: Summary of surface and crystallographic information of SiO_2/Si thin film samples

Sample No.	Roughness R_a (nm)	Peak position θ/2θ (degree)	Peak intensity (cps)
Sample 1	14.0	27.6	216
Sample 2	14.3	28.7	240
Sample 3	15.2	29.9	177
Sample 4	13.6	29.2	259.5
Sample 5	13.8	29.6	149.5
Sample 6	15.0	28.1	173
Sample 7	13.0	28.2	134
Sample 8	13.4	27.5	209.5
Sample 9	14.4	27.5	181.5

A regression model was derived in case a thin film with a particular roughness is desired. The model summary of the regression analysis is listed in table 5.

$$\text{Roughness } (R_a)\text{ (nm)} = \begin{array}{l} 14.782 - 0.01350 \text{ Power (Watt)} \\ + 0.1677 \text{ Pressure (mTorr)} \\ - 0.0183 \text{ Ar Gas Flow (sccm)} \end{array} \quad (6)$$

Table 5: Model summary of the regression analysis of surface roughness of SiO_2/Si thin films

S	R-sq	R-sq(adj)	R-sq(pred)
0.211100	96.92%	95.06%	89.14%

3.2 Crystallography and Morphology

The XRD patterns of the SiO_2/Si thin film samples (sample 1-sample 9) is shown in Figure 2. No peak was detected in all sample scanned from position θ=20° to θ=65°, which led to the conclusion that the deposited SiO_2 layers were amorphous. According to PDF #81-0066 card, if the layered SiO_2 film was crystallized, there would be some conspicuous peaks at θ = 27.3° or θ = 21.6°, indicating quartz (011) or (100) plane respectively [7], which was not the case. A strong peak was detected at position θ=69.1° for each of the samples, but this peak is related to the Si (100) substrate. The amorphous deposited layers of SiO_2 were also reported in previous literature [7, 15]. The XRD peak intensities in count per second (cps) and peak positions of each sample were tabulated in table 4. Peak positions were obtained between θ= 27.5° to 29.9° range and peak intensities varied arbitrarily from 134 cps (sample 7) to 259.5 cps (sample 4), following no trend. Because of these amorphous XRD patterns, no further information like grain size and micro stress could be derived for the nine SiO_2/Si thin film samples.

Downloaded from http://asmedigitalcollection.asme.org/IMECE/proceedings-pdf/IMECE2021/85574/V003T03A039/6827069/v003t03a039-imece2021-73849.pdf by Texas A & M University user on 23 January 2023

Copyright © 2021 by ASME

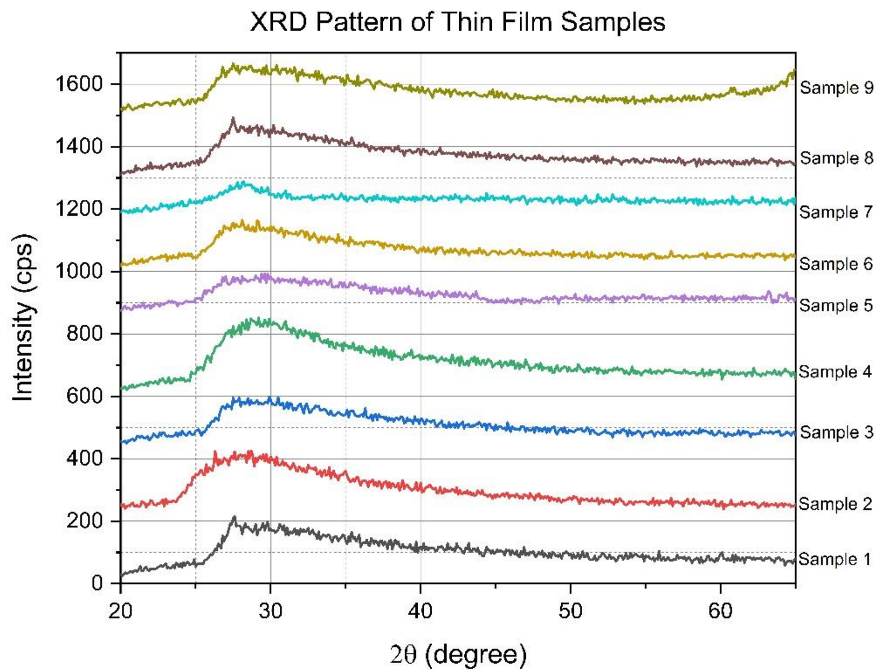

FIGURE 2: XRD PATTERN OF SiO2/Si THIN FILM SAMPLES PRESENTED IN STACKED LINES BY Y OFFSET

Table 6: Summary of ANOVA result for surface roughness (R_a) of SiO_2/Si thin film samples

Source	DF	Seq SS	Contribution	Adj SS	Adj MS	F-Value	P-Value
Power (Watt)	2	2.73620	37.88%	2.73620	1.36810	27.96	0.035
Pressure (mTorr)	2	4.33687	60.04%	4.33687	2.16843	44.31	0.022
Ar Gas Flow (sccm)	2	0.05287	0.73%	0.05287	0.02643	0.54	0.649
Error	2	0.09787	1.35%	0.09787	0.04893		
Total	8	7.22380	100.00%				

Figure 4 depicts surface and cross-sectional SEM images of samples 3,4 and 8 of SiO_2/Si thin films. The surface of sample 3 displayed no ditches, whereas ditch-like morphology appeared on the surface of samples 4 and 8. No pronounced granular shape was noticed in all three samples. This kind of surface morphology was also described in Zhao et al. [7]. Although Zhao et al. attributed the presence of ditches on the sample surface to the decreasing process gas pressure, in this observation, however, the contribution of sputtering power was more profound. Trenches appeared most clearly on the surface of sample 8, which was deposited with the highest RF sputtering power (250 Watt). Sample 4 deposited with 200 Watt RF power showed less visible ditches. SEM cross-sectional images did not provide enough information. One reason for this was the deposited layers were not thick enough for the micro-structures to be visible. The cross-sectional SEM image of sample 8 vaguely showed domain-like shapes with no columnar microstructure. 2D and 3D AFM images of surface topographies of samples 3, 4 and 8 are shown in Figure 5.

3.3 Electrical Properties

Electrical properties (resistance per unit area R_{nA} and capacitance per unit area C_{nA}) of SiO2/Si thin films were examined with impedance spectroscopy.

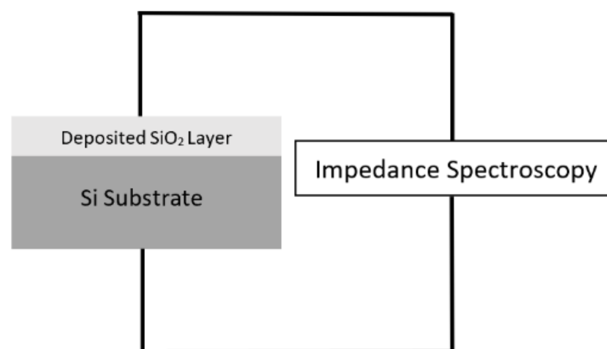

FIGURE 3: CONNECTION DIAGRAM SiO2/SI THIN FILM SAMPLES FOR IMPEDANCE SPECTROSCOPY MEASUREMENT

Downloaded from http://asmedigitalcollection.asme.org/IMECE/proceedings-pdf/IMECE2021/85574/V003T03A039/6827069/v003t03a039-imece2021-73849.pdf by Texas A & M University user on 23 January 2023

Copyright © 2021 by ASME

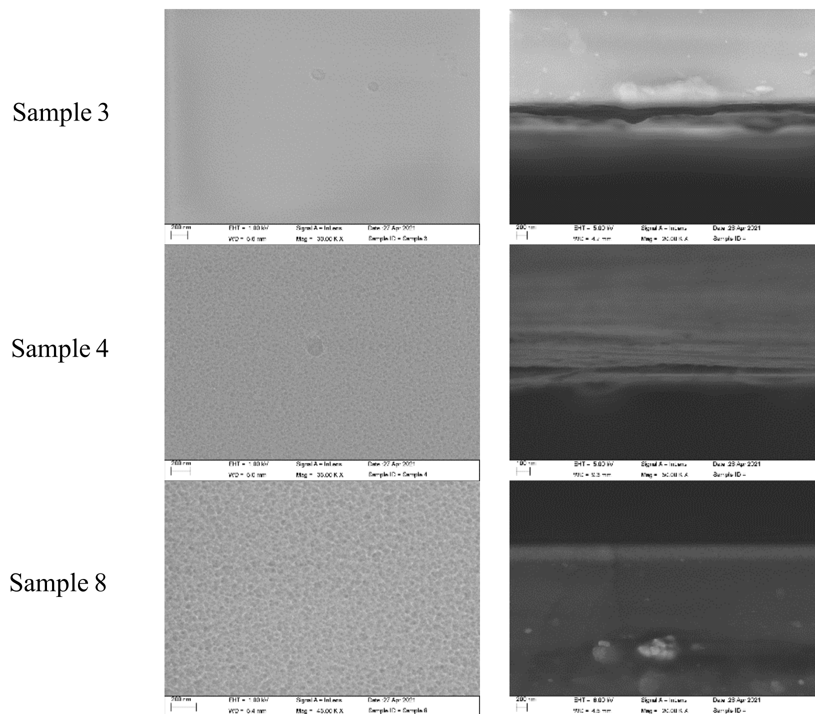

FIGURE 4: SURFACE (LEFT) AND CROSS-SECTIONAL (RIGHT) SEM MICROGRAPH OF THE SiO_2/Si THIN FILM SAMPLES

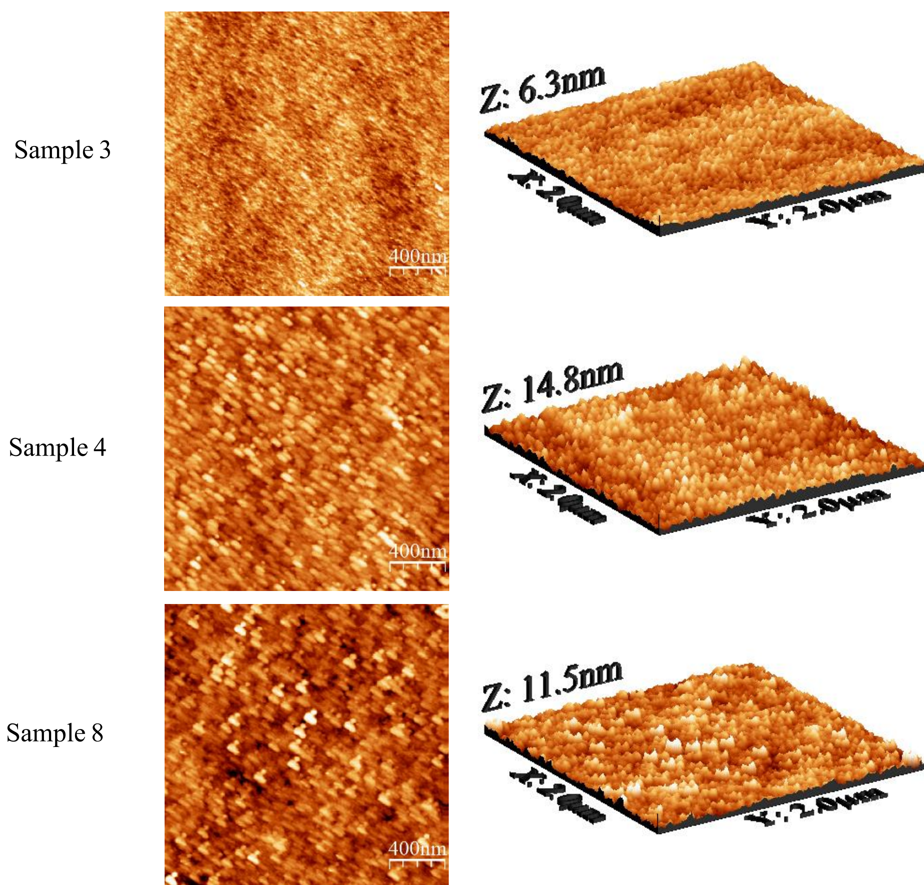

FIGURE 5: AFM IMAGES (LEFT 2D AND RIGHT 3D) OF THE SiO_2/Si THIN FILM SAMPLES

Copyright © 2021 by ASME

Downloaded from http://asmedigitalcollection.asme.org/IMECE/proceedings-pdf/IMECE2021/85574/V003T03A039/6827069/v003t03a039-imece2021-73849.pdf by Texas A & M University user on 23 January 2023

Impedance spectroscopy gives bode plot (impedance Z_n & phase angle vs. frequency) and nyquist plot (Z_n (img) vs. Z_n (real)) of the films. Z_n (real) can be attributed to resistance R_n of the thin film and the capacitance of the SiO_2/Si thin film contributes to the Z_n (img) part of the impedance spectroscopy. To get the resistance and capacitance of the nth sample, we used the following equations.

$$R_n = Z_n(real)$$
$$C_n = \frac{1}{2\pi f Z_n(img)} \tag{7}$$

Where f is the frequency. Now, as from the connection in Figure 3, the deposited SiO_2 superstrate and the Si substrate are in series. So, we can write the following equations:

$$R_n = R_{Si} + R_{nSiO_2}$$
$$\frac{1}{C_n} = \frac{1}{C_{Si}} + \frac{1}{C_{nSiO_2}} \tag{8}$$

Further we can write:

$$\frac{R_n}{A_n} = \frac{R_{Si}}{A_n} + \frac{R_{nSiO_2}}{A_n}$$

Or,

$$R_{nA} = \frac{R_{Si}}{A_n} + \frac{R_{nSiO_2}}{A_n}$$

And,

$$\frac{1}{\frac{C_n}{A_n}} = \frac{1}{\frac{C_{Si}}{A_n}} + \frac{1}{\frac{C_{nSiO_2}}{A_n}} \tag{9}$$

Or,

$$\frac{1}{C_{nA}} = \frac{1}{\frac{C_{Si}}{A_n}} + \frac{1}{\frac{C_{nSiO_2}}{A_n}}$$

Now, R_{Si} and C_{Si} are both constant for a particular frequency, which makes $\frac{R_{Si}}{A_n}$ and $\frac{C_{Si}}{A_n}$ also constant. Thus, for a particular frequency, the changes of R_n and C_n are simply due to the change in R_{nSiO_2} and C_{nSiO_2}. Process parameters variation during sputtering changes the structure of the deposited SiO_2 thin film over Si substrate and therefore, the electrical properties of the thin films change with it. Each sample was deposited for 3hours, so deposition time was not a parameter for our observation.

Figure 6 shows the resistance/area (R_{nA}) and capacitance/area (C_{nA}) vs. frequency plots for sample 1-9. Normalizing with sample area (A_n) was intentionally carried out to omit the area difference effect on the electrical properties. In all cases, R_{nA} and C_{nA} decreased with increasing frequency. The rate of decline of R_{nA} with frequency was not always the same for the SiO_2/Si thin film samples and R_{nA} vs. frequency curves can be divided into three regions. The first region where R_{nA} drops steeply ranges from 1Hz to about 300 Hz. This rate slowed down in the second region ranging from 300Hz to about 70kHz, then again fell down faster in somewhat about 70kHz to 1MHz range. Although, R_{nA} vs. frequency curves of all samples showed these three regions, however, the rate of decrease and the range limit of frequency in the mentioned three regions of the R_{nA} vs. frequency curve varies from sample to sample. From the C_{nA} vs. frequency plots of the thin film samples, it was observed that at higher frequency (>7kHz), the decrease rate of C_{nA} with frequency was less than that at lower frequencies. Also, similar to R_{nA} vs. frequency curves, the decline rate of C_{nA} with frequency varied in each sample.

Table 7 shows R_{nA} and C_{nA} at 50kHz and 10kHz. Data at 50 kHz was used to analyze Taguchi DOE. In this region, as shown in Figure 6, the data is more trending with lesser outliers. S/N graphs for electrical properties of the SiO_2/Si thin film samples are shown in Figure 7 and the ANOVA results for resistance/area (R_{nA}) and capacitance/area (C_{nA}) are tabulated in Table 8 and 9, respectively. Taguchi analysis for 10kHz was also performed, which showed almost similar results as Figure 7, but the ANOVA analysis for resistance/area (R_{nA}) resulted in P-value>0.05 (sputtering power had the smallest P-value=0.157) for each of the parameters and it is not presented in this paper.

In order to explain the S/N graph in Figure 7, we first look at what changes the electrical properties SiO_2/Si thin films. Here two factors are influencing R_{nA} and C_{nA}. The first one is the layer thickness d_n and the other is the number of nucleation sites on the substrate surface and nucleation growth, or, in different words, the amount of micro-voids and pores present in the thin film structures. Note that the substrate thickness d_{Si} is constant. The layer thickness d_n of the thin films is a function of process parameters, so SiO_2 layer thicknesses vary from sample to sample.

Table 7: Summary of Electrical Properties of SiO_2/Si thin film samples

Sample No.	R_{nA} at 50kHz (Ω/cm^2)	C_{nA} at 50kHz ($\mu F/cm^2$)	R_{nA} at 10kHz (Ω/cm^2)	C_{nA} at 10kHz ($\mu F/cm^2$)
Sample 1	2.69×10^4	5.24×10^{-6}	4.82×10^4	5.83×10^{-6}
Sample 2	3.48×10^4	5.92×10^{-6}	6.16×10^4	6.60×10^{-6}
Sample 3	2.81×10^4	6.12×10^{-6}	5.62×10^4	6.95×10^{-6}
Sample 4	1.44×10^4	6.56×10^{-6}	3.13×10^4	7.01×10^{-6}
Sample 5	2.75×10^4	7.49×10^{-6}	4.54×10^4	8.56×10^{-6}
Sample 6	1.93×10^4	7.24×10^{-6}	3.35×10^4	8.43×10^{-6}
Sample 7	2.62×10^4	3.69×10^{-6}	5.62×10^4	3.96×10^{-6}
Sample 8	3.52×10^4	4.75×10^{-6}	5.59×10^4	5.17×10^{-6}
Sample 9	2.16×10^4	4.06×10^{-6}	3.38×10^4	4.46×10^{-6}

Downloaded from http://asmedigitalcollection.asme.org/IMECE/proceedings-pdf/IMECE2021/85574/V003T03A039/6827069/v003t03a039-imece2021-73849.pdf by Texas A & M University user on 23 January 2023

Copyright © 2021 by ASME

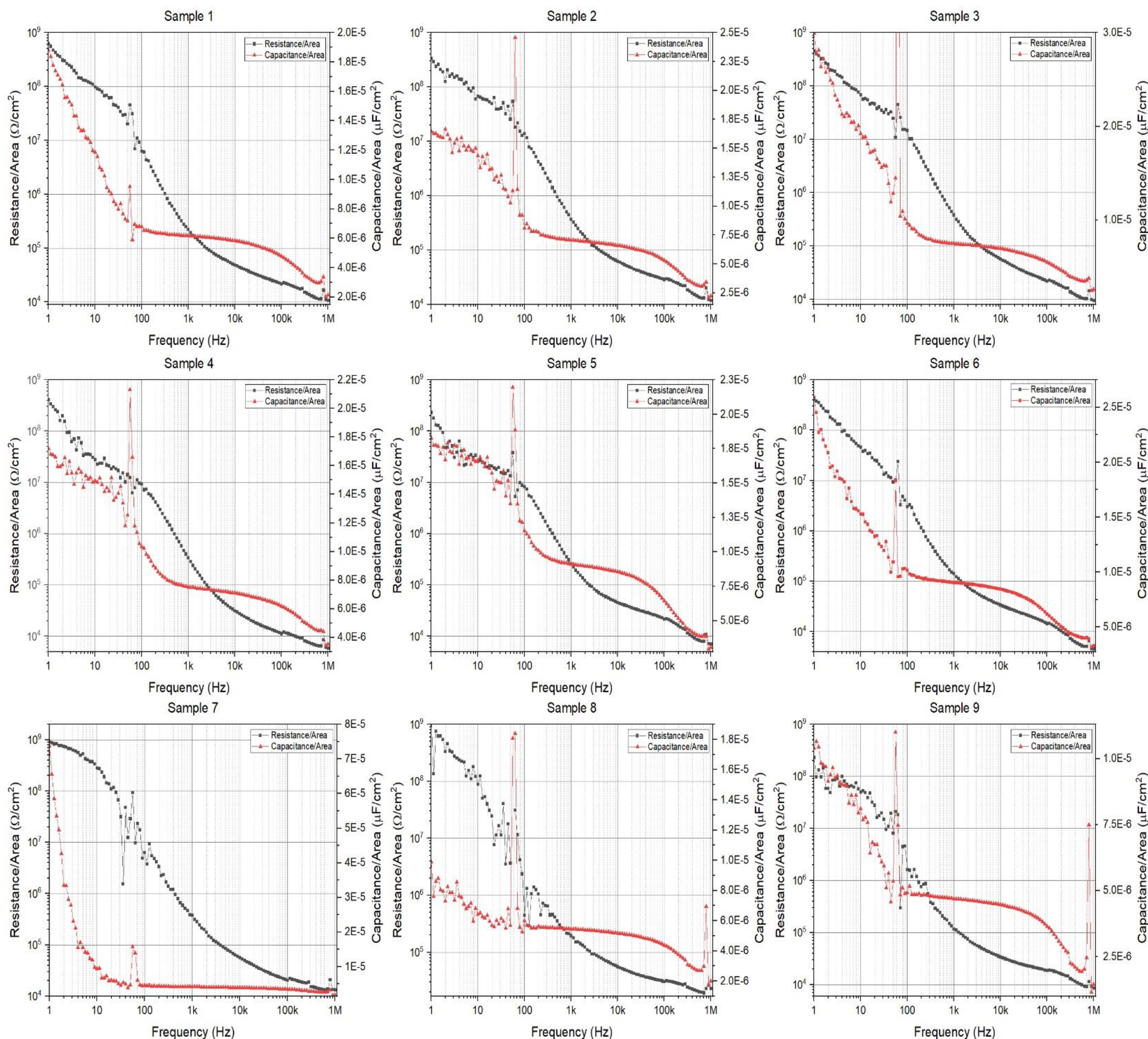

FIGURE 6: RESISTANCE/AREA (R_{nA}) AND CAPACITANCE/AREA (C_{nA}) VS. FREQUENCY PLOTS FOR SiO_2/Si THIN FILM SAMPLES

Increasing the sputtering power creates more nucleation sites on the surface of the substrate [32]. Because of the high kinetic energy of the falling target atoms at higher power, more atoms can reach the surface initially and act as nucleation sites. The deposition rate increases with sputtering power as well [6]. The resistance of the thin film is directly proportional and the capacitance is inversely proportional to the layer thickness d_n. When the sputtering power begins to rise, increased nucleation sites on the substrate surface and higher nucleation growth start to fill up the micro-voids and cavities in the layer structure faster than the deposition rate. In this period, the resistance of the deposited layer decreases and capacitance increases. However, increasing power only boosts the deposition rate after a certain power range, as the number of nucleation sites on the surface strats to saturate. So, this event forces the resistance to go up and capacitance to go down as the growing layer thickness is the dominating factor now. This is why S/N for R_{nA} decreased and S/N for C_{nA} increased first. After 200W, escalating power reduced C_{nA}, but R_{nA} improved. The effect of pressure on the R_{nA} of the thin films should be the opposite. Because of the shrunk mean free path, increased inter-atomic collisions between target and process gas atoms at higher pressure impede the target atom from reaching the substrate surface and acting as nucleation sites. Consequently, nucleation growth slows down, deposited

Downloaded from http://asmedigitalcollection.asme.org/IMECE/proceedings-pdf/IMECE2021/85574/V003T03A039/6827069/v003t03a039-imece2021-73849.pdf by Texas A & M University user on 23 January 2023

Copyright © 2021 by ASME

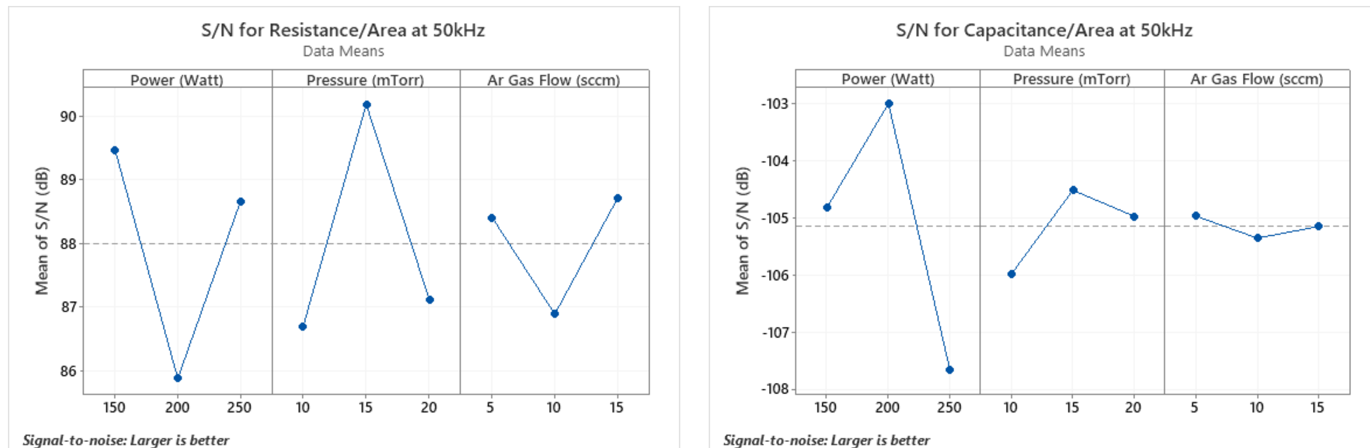

FIGURE 7: S/N GRAPH FOR THE ELECTRICAL PROPERTIES OF THE SiO_2/Si THIN FILMS; (LEFT) RESISTANCE/AREA (R_{nA}) AND CAPACITANCE/AREA (C_{nA}) (RIGHT) AT 50 kHz.

Table 8: Summary of ANOVA result for RESISTANCE/AREA (R_{nA}) at 50 kHz frequency for SiO_2/Si thin films

Source	DF	Seq SS	Contribution	Adj SS	Adj MS	F-Value	P-Value
Power (Watt)	2	1.48E+8	40.40%	1.48E+8	7.44E+7	47.60	0.021
Pressure (mTorr)	2	1.90E+8	51.71%	1.90E+8	9.52E+7	60.93	0.016
Ar Gas Flow (sccm)	2	2.59E+7	7.04%	2.59E+7	1.30+7	8.30	0.108
Error	2	3.13E+6	0.85%	3.13E+6	1.56E+7		
Total	8	3.68E+8	100.00%				

Table 9: Summary of ANOVA result for CAPACITANCE/AREA (C_{nA}) at 50 kHz frequency for SiO_2/Si thin films

Source	DF	Seq SS	Contribution	Adj SS	Adj MS	F-Value	P-Value
Power (Watt)	2	0.000000	89.79%	0.000000	0.000000	155.01	0.006
Pressure (mTorr)	2	0.000000	8.81%	0.000000	0.000000	15.21	0.062
Ar Gas Flow (sccm)	2	0.000000	0.82%	0.000000	0.000000	1.41	0.415
Error	2	0.000000	0.58%	0.000000	0.000000		
Total	8	0.000000	100.00%				

layers become less dense with full of voids and gaps and produce highly resistive films. A lower deposition rate at high pressure also leads to thinner films. As a result, rising the pressure from 10mTorr to 15 mTorr improved both R_{nA} and C_{nA}. However, from the pressure range 15mTorr to 20mTorr, R_{nA} and C_{nA} both degrade. In this pressure range, reducing film thicknesses affecting R_{nA} more and the influecne of excessive micro-voids in the layer structure on the relative permittivity overcomes the impact of the shortening film thickness d_n on the capacitance of the film, which in consequence, decrease C_{nA}.

The ANOVA analysis in Table 8 reveals working pressure has the highest contribution on R_{nA} (51.71%). Power has slightly less contribution 40.40%. Both of the contributions are significant. For C_{nA}, power is the dominant factor (contribution 89.79%) in contrast to pressure contribution (8.81%). The contribution of Ar gas flow rate can be ignored as it is not very significant (7.04% for R_{nA} and 0.82% for C_{nA} and in both cases P-value > 0.05). The non-linear behavior of the S/N graphs for the electrical properties of the SiO_2/Si thin films is the reason why no regression model could not be derived for resistance/area (R_{nA}) and capacitance/area (C_{nA}).

The adhesion of the SiO_2/Si thin films was examined by scotch tape test. All nine samples passed the adhesion test. They remain adhered to the substrate even after pulling off the tape.

4. CONCLUSION

SiO_2 thin film samples were deposited over Si substrate by radio frequency (RF) magnetron sputtering system. Taguchi DOE and ANOVA analysis were performed to understand the effect of three process parameters-power, pressure and Ar gas flow rate and their individual contribution on surface, morphological and electrical properties of the SiO_2/Si thin films.

Downloaded from http://asmedigitalcollection.asme.org/IMECE/proceedings-pdf/IMECE2021/85574/V003T03A039/6827069/v003t03a039-imece2021-73849.pdf by Texas A & M University user on 23 January 2023

Copyright © 2021 by ASME

It was determined that power and pressure are the dominant factors that influence the significant percentage of the properties in most cases. Ar gas flow rate has little effect on the properties of the sputtered SiO_2/Si thin films.

ACKNOWLEDGEMENTS

This research was supported by Major Research Instrument (MRI) program under National Science Foundation (NSF). Also, the authors are thankful to our colleagues- Muhtasim Ul Karim Sadaf, KIM Iqbal and Dr. Victoria Pallida for helping us perform this research.

Special mention-Al Mazedur Rahman. He contributed massively in surface roughness measurement and Taguchi and ANOVA statistical analysis. Without his cooperation, it would not be possible for us to complete this paper neatly. We would like to add his name in the author list.

REFERENCES

1. Pierson, H., O., *Handbook of Chemical Vapor Deposition (CVD)*. 2nd ed. Principles, Technology and Applications. Park Ridge, New Jersey, USA: Noyes Publications.
2. Robles, S., E. Yieh, and B. Nguyen, C., *Moisture resistance of plasma enhanced chemical vapor deposited oxides used for ultra-large scale integrated device applications.* Journal of The Electrochemical Society, 1995. **142**: p. 580-585.
3. Cao, Z., T.-Y. Zhang, and X. Zhang, *Microbridge testing of plasma-enhanced chemical-vapor deposited silicon oxide films on silicon wafers.* Journal of Applied Physics, 2005. **97**(10).
4. Jaecklin, V., P., et al., *Line-addressable torsional micromirrors for light modulator arrays.* Sensors and Actuators A: Physical, April 1994. **41**(1-3): p. 324-329.
5. Tang, W., C., T. Nguyen, C., H., and R. Howe, T. *Laterally driven polysilicon resonant microstructures*. in *IEEE International Conference on Micro Electro Mechanical Systems*. 1989. Salt Lake City, UT, USA: IEEE.
6. Bhatt, V. and S. Chandra, *Silicon dioxide films by RF sputtering for microelectronic and MEMS applications.* Journal of Micromechanics and Microengineering, 2007. **17**(5): p. 1066-1077.
7. Zhao, L., et al., *Effect of sputtering pressure on the structure and properties of SiO2 films prepared by magnetron sputtering.* Micro & Nano Letters, 2020. **15**(12): p. 872-876.
8. Kanmaz, İ. and A. ÜZÜM, *Silicon dioxide thin films prepared by spin coating for the application of solar cells.* International Advanced Researches and Engineering Journal, 2021. **5**(1): p. 14-18.
9. Ho, W.J., et al., *Electrical and Optical Characterization of Sputtered Silicon Dioxide, Indium Tin Oxide, and Silicon Dioxide/Indium Tin Oxide Antireflection Coating on Single-Junction GaAs Solar Cells.* Materials (Basel), 2017. **10**(7).
10. Jiang, Y., et al., *Optical and interfacial layer properties of SiO2 films deposited on different substrates.* Appl Opt, 2014. **53**(4): p. A83-7.
11. Yang, Y., et al., *Preparation of a novel TiN/TiNxOy/SiO2 composite ceramic films on aluminum substrate as a solar selective absorber by magnetron sputtering.* Journal of Alloys and Compounds, 2020. **815**.
12. Bartzsch, H., et al., *Properties of SiO2 and Al2O3 films for electrical insulation applications deposited by reactive pulse magnetron sputtering.* Surface and Coatings Technology, 2003. **174-175**: p. 774-778.
13. Choi, B.J., et al., *Purely electronic switching with high uniformity, resistance tunability, and good retention in Pt-dispersed SiO2 thin films for ReRAM.* Adv Mater, 2011. **23**(33): p. 3847-52.
14. Tahir, D., et al., *Electronic and optical properties of Al2O3/SiO2thin films grown on Si substrate.* Journal of Physics D: Applied Physics, 2010. **43**(25).
15. Jeong, S.-H., et al., *Characterization of SiO2 and TiO2 films prepared using rf magnetron sputtering and their application to anti-reflection coating.* Vacuum, 2004. **76**(4): p. 507-515.
16. Wu, W.-F. and B.-S. Chiou, *Optical and mechanical properties of reactively sputtered silicon dioxide films.* Semiconductor Science and Technology, 1996. **11**(9): p. 1317-1321.
17. Bartzsch, H., et al., *Electrical insulation properties of sputter-deposited SiO2, Si3N4and Al2O3films at room temperature and 400 °C.* physica status solidi (a), 2009. **206**(3): p. 514-519.
18. Hanby, B.V.T., et al., *Layered Al2O3-SiO2 and Al2O3-Ta2O5 thin-film composites for high dielectric strength, deposited by pulsed direct current and radio frequency magnetron sputtering.* Applied Surface Science, 2019. **492**: p. 328-336.
19. Kawasaki, H., et al., *Preparation of Sn doped SiO2thin films by magnetron sputtering deposition using metal and metal-oxide powder targets.* Japanese Journal of Applied Physics, 2019. **58**(SA).
20. Hsu, H.-L., et al., *Electrical and optical studies of Ga-doped ZnO thin films.* Journal of Materials Science: Materials in Electronics, 2012. **24**(1): p. 13-19.
21. Huang, P.-c., et al., *The Effect of Sputtering Parameters on the Film Properties of Molybdenum Back Contact for CIGS Solar Cells.* International Journal of Photoenergy, 2013. **2013**: p. 1-8.
22. Cesiulis, H., et al., *The Study of Thin Films by Electrochemical Impedance Spectroscopy*, in *Nanostructures and Thin Films for Multifunctional Applications*. 2016. p. 3-42.
23. Chaik, M., et al., *Analysis of the electrical impedance spectroscopy measurements of ZnTe:Ni thin film*

Downloaded from http://asmedigitalcollection.asme.org/IMECE/proceedings-pdf/IMECE2021/85574/V003T03A039/6827069/v003t03a039-imece2021-73849.pdf by Texas A & M University user on 23 January 2023

Copyright © 2021 by ASME

deposited by R–F sputtering. Superlattices and Microstructures, 2020. **137**.
24. Dabbabi, S., et al., *Effects of Ni and La Dopants on the Properties of ZnO and SnO2 Thin Films: Microstructural, Optical and Impedance Spectroscopy Studies.* Journal of Electronic Materials, 2019. **49**(2): p. 1314-1321.
25. Erinmwingbovo, C., et al., *Dynamic impedance spectroscopy of LiMn2O4 thin films made by multi-layer pulsed laser deposition.* Electrochimica Acta, 2020. **331**.
26. Kao, P.S. and H. Hocheng, *Optimization of electrochemical polishing of stainless steel by grey relational analysis.* Journal of Materials Processing Technology, 2003. **140**(1-3): p. 255-259.
27. Yang, W., H. and Y. Tarng, S., *Design optimization of cutting parameters for turning operations based on the Taguchi metho.* Journal of Materials Processing Technology, 1998. **84**(1-3): p. 122-129.
28. Minitab® 18 Support. *What is the signal-to-noise ratio in a Taguchi design?* ; Available from: https://support.minitab.com/en-us/minitab/18/help-and-how-to/modeling-statistics/doe/supporting-topics/taguchi-designs/what-is-the-signal-to-noise-ratio/.
29. Minitab® 18 Support. *Model summary table for Fit Regression Model*. Available from: https://support.minitab.com/en-us/minitab/18/help-and-how-to/modeling-statistics/regression/how-to/fit-regression-model/interpret-the-results/all-statistics-and-graphs/model-summary-table/.
30. Wu, H.-M., et al., *Structure and electrical properties of Mo back contact for Cu(In, Ga)Se2 solar cells.* Vacuum, 2012. **86**(12): p. 1916-1919.
31. Badgujar, A.C., S.R. Dhage, and S.V. Joshi, *Process parameter impact on properties of sputtered large-area Mo bilayers for CIGS thin film solar cell applications.* Thin Solid Films, 2015. **589**: p. 79-84.
32. Le, M.-T., et al., *Effect of Sputtering Power on the Nucleation and Growth of Cu Films Deposited by Magnetron Sputtering.* Materials Transactions, 2010. **51**(1): p. 116-120.

Downloaded from http://asmedigitalcollection.asme.org/IMECE/proceedings-pdf/IMECE2021/85574/V003T03A039/6827069/v003t03a039-imece2021-73849.pdf by Texas A & M University user on 23 January 2023

Copyright © 2021 by ASME